JOURNAL OF MATERIALS SCIENCE **40** (2005) 4061 – 4066

Hydrogen permeability and effect of microstructure on mixed protonic-electronic conducting Eu-doped strontium cerate

S.-J. SONG*,†, E. D. WACHSMAN, J. RHODES, H.-S. YOON, K.-H. LEE, G. ZHANG
Dept. of Materials Science and Engineering, University of Florida, Gainesville, FL 32611, USA
E-mail: song@anl.gov

S. E. DORRIS, U. BALACHANDRAN
Argonne National Laboratory, Energy Technology Division, Argonne, IL 60439, USA

The hydrogen permeability of $SrCe_{0.95}Eu_{0.05}O_{3-\delta}$ was studied as a function of temperature, hydrogen partial pressure (P_{H_2}) gradient, and water vapor partial pressure (P_{H_2O}) gradient. The effect of the microstructure on hydrogen permeability through a 1.72 mm thick membrane was investigated. The ambipolar conductivity calculated from hydrogen permeation fluxes showed the same P_{O_2} and P_{H_2} dependence as the electronic conductivity, for the experimental conditions. The small grained membrane showed higher hydrogen permeability when compared with the larger grained membrane over the entire temperature range investigated.

1. Introduction

A growing attention in the development of an environmentally benign, inexpensive technology for separating hydrogen from water [1, 2] and/or syngas [3, 4] has motivated the research on proton conductors. Significant researches on proton conducting oxide have been performed over various chemical structures [5–7]. Among them, perovskite structure oxide is still preferably chosen as a prototype material for investigating its transport properties and defect structure due to the growing importance of this oxide for the use of hydrogen separation membranes, sensors, and fuel cells applications [8–11]. Especially, proton transport properties in multivalent cation-substituted strontium cerate have been studied over a number of years in our group for hydrogen separation membrane application due to the high proton selectivity and the low oxygen ion conductivity of strontium cerate. Furthermore, separation process is purely ion transport, not physically that they produce nearly 100% pure hydrogen. They also function nongalvanically, i.e., without electrodes or external electrical circuitry.

Among them, Europium, in this study, was doped to strontium cerate because of the electronic conductivity provided by the multivalent europium dopant [12]. Its defect structure and defect related material properties were studied for monolithic hydrogen separation membrane applications [13, 14].

In this work, the hydrogen permeability of $SrCe_{0.95}Eu_{0.05}O_{3-\delta}$ were studied as a function of temperature, P_{O_2}, P_{H_2}, and P_{H_2O}. Based on chemical diffusion theory, ambipolar conductivities at given thermodynamic conditions were calculated. Microstructure effect on hydrogen permeability was also discussed.

2. Theory

Assuming a fixed Sr/(Ce + Eu) ratio, the defect structure of multivalent cation doped strontium cerate may be well described by the irregular structure elements (such as electron (e'), hole($h^{\cdot}$), oxygen vacancies ($V_o^{\cdot\cdot}$), proton ($OH_o^{\cdot}$), cation vacancies (V_{Sr}'', V_{Ce}''''), and acceptor dopant (Eu'_{Ce}, Eu''_{Ce})) and by the external and internal equilibria. Mass action laws are applied to defect equilibria and Kroger-Vink notation is used [15].

(a) Internal equilibria

$$null = V_{Sr}'' + V_{Ce}'''' + 3V_O^{\cdot\cdot}; \quad K_s = [V_{Sr}''][V_{Ce}''''][V_O^{\cdot\cdot}]^3 \tag{1}$$

*Author to whom all correspondence should be addressed.
†*Present address*: Ceramics Section, Energy Technology Division, Argonne National Laboratory 9700 South Cass Ave. Argonne, IL 60439, USA.

where K_s is the equilibrium constant for Schottky-Wagner disorder.

$$null = e' + h^{\cdot}; \quad K_i = n \cdot p \tag{2}$$

where K_i is the equilibrium constant for electron-hole pair intrinsic reaction. n and p is electron and hole concentration, respectively.

(b) External equilibria

$$O_O^x \rightarrow \frac{1}{2}O_2(g) + V_O^{\cdot\cdot} + 2e'; K_R = [V_O^{\cdot\cdot}]n^2 p_{O_2}^{1/2} \tag{3}$$

where K_R is the equilibrium constant for exchange of oxygen.

$$H_2O(g) + V_O^{\cdot\cdot} + O_O^x \rightarrow 2OH_O^{\cdot}; K_W = \frac{[OH_O^{\cdot}]^2}{[V_O^{\cdot\cdot}]P_{H_2O}} \tag{4}$$

where K_W is the equilibrium constant for exchange of water.

(c) Ionization equilibrium of doped Yb

$$Eu'_{Ce} \rightarrow Eu''_{Ce} + h^{\cdot}; K_A = \frac{[Eu''_{Ce}] \cdot p}{[Eu''_{Ce}]} \tag{5}$$

where K_A is the equilibrium constant for europium ionization reaction.

(d) Charge neutrality condition

$$n + 2[Eu''_{Ce}] + [Eu'_{Ce}] = p + 2[V_O^{\cdot\cdot}] + [OH_O^{\cdot}] \tag{6}$$

The possibility of interstitial disorders is ruled out because they are energetically unfavourable in the perovskite structure from a structural viewpoint [16].

Once a hydrogen chemical potential gradient is applied, hydrogen will permeate due to the nature of ambipolar diffusion of proton and electrons determined by defect equilibria. As the characteristics of hydrogen separation membranes severely count on the overall kinetics of the membrane oxides, overall kinetics of hydrogen permeation is a key information to optimizing the membrane devises. The overall hydrogen permeation process consists largely of three consecutive kinetic steps: gas/solid interfacial reaction, solid-state diffusion, and solid/gas interfacial reaction. For the $SrCe_{1-x}Yb_xO_{3-d}$ system, however, it has been reported in permeation studies at elevated temperature that the surface exchange reaction kinetics be fast enough, and overall kinetics is primarily governed by the solid-state diffusion step above 2 micrometer thick membrane [17]. Therefore, permeation through 1.72-mm-thick $SrCe_{1-x}M_xO_{3-\delta}$ membranes (the thickness we used in experiments reported in this paper) should be bulk diffusion controlled. By assuming bulk diffusion, the hydrogen permeation flux across an oxide membrane can be derived by the Wagner equation [18].

$$2J_{H_2} = J_{OH_O^{\cdot}} = -\frac{1}{L}\left\{\frac{RT}{4F^2}\int_{P'_{O_2}}^{P''_{O_2}} \sigma_t t_{OH_O^{\cdot}} t_{v_O^{\cdot\cdot}} d\ln P_{O_2} + \frac{RT}{2F^2}\int_{P'_{H_2}}^{P''_{H_2}} \sigma_t t_{OH_O^{\cdot}}\left(t_{V_O^{\cdot\cdot}} + t_{e'}\right) d\ln P_{H_2}\right\} \tag{7}$$

where σ_t is the total conductivity, t_i is the transference number of the charged species ($I = OH_O^{\cdot}, V_O^{\cdot\cdot}, e'$), L is thickness of membrane, F is the Faraday constant $d\ln P_{O_2}$ $d\ln P_{H_2}$ are the chemical potential gradients across an oxide membrane.

3. Experimental

Polycrystalline $SrCe_{0.95}Eu_{0.05}O_{3-\delta}$ samples were prepared by conventional solid-state reaction methods. High-purity oxide powders of $SrCO_3$ (99.9% Alfa Aesar), and CeO_2 (99.9% Alfa Aesar) were mixed with Eu_2O_3 (99.99%, Alfa Aesar), ground in a ball mill with stabilized zirconia balls in ethanol, and calcined at 1573 K for 10 h in air. To investigate the effect of microstructure on hydrogen permeation, membranes were prepared in different ways. The calcined oxides were then crushed, sieved to <45 microns, ground in a ball mill again for 1 and 5 days, pressed into pellets, cold-isostatic-pressed at 200 MPa, and sintered at 1773 K for 10, 25, and 40 hrs in air. The densities of the resultant disks were above 94% of theoretical. X-ray diffraction spectra confirmed that all specimens obtained in this way exhibit a single phase of the orthorhombic perovskite structure.

Microscopic investigations of three membranes (after thermally etched at 1773 K for 1 hr) were made by scanning electron micrographs (Model 6300, JEOL, Tokyo, Japan), as shown in Fig. 1. One membrane ball milled for 10 days and sintered at 1773 K for 10 hrs, Fig. 1a, showed small and narrow grain size distribution. Another membrane ball milled for 1 day and sintered at 1773 K for 25 hrs, Fig. 1b, showed some pores and irregular grain size distribution due to the short ball milling time. The other membrane ball milled for 1 day and sintered at 1773 K for 40 hrs, Fig. 1c, showed very dense microstructure.

Hydrogen permeation was measured on dense disk 24 mm in diameter × 1.72 mm thick. The planar surfaces of each disk were polished with 1200-grit SiC paper. Polished disks were sealed with ceramic sealant to alumina tubes. The sweep side flow was a constant 20 sccm of helium; the feed gas flow, 50 sccm of H_2/Ar mixtures. For wet gas flow, feed gas mixture was bubbled through a water bath at room temperature. The hydrogen content of the permeate stream was measured with Q100MS Dycor Quadlink mass spectrometer. Leakage of neutral gas through pores in the sample or through an incomplete seal was checked by measuring the argon tracer content of the permeate stream. No discernible leak was detected. Comprehensive experimental details will be discussed in a future publication.

4. Results and discussion

4.1. Hydrogen permeation fluxes

From the hydrogen content measured in the helium sweep side of the permeation assembly and the helium flow rate, the total hydrogen permeation rate (mol/sec) was calculated, while assuming the ideal gas law. Then, the permeation fluxes (mol/cm^{2}sec) were calculated by

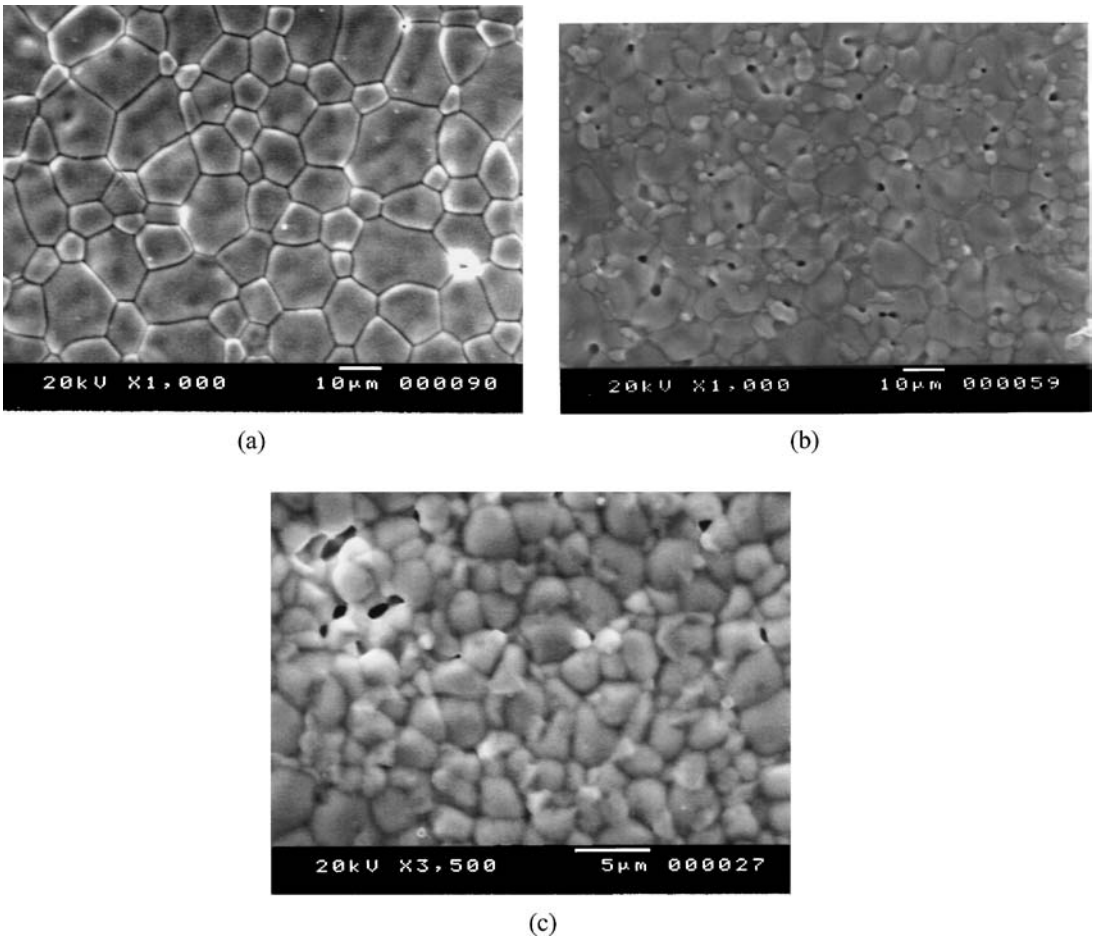

Figure 1 Scanning electron micrographs of $SrCe_{0.95}Eu_{0.05}O_{3-d}$ membranes after being thermally etched. (a) ball mill for 1 days and sintered at 1773 K for 40 hrs, (b) ball mill for 1 days and sintered at 1773 K for 25 hrs, (c) ball milled for 10 days and sintered at 1773 K for 10 hrs.

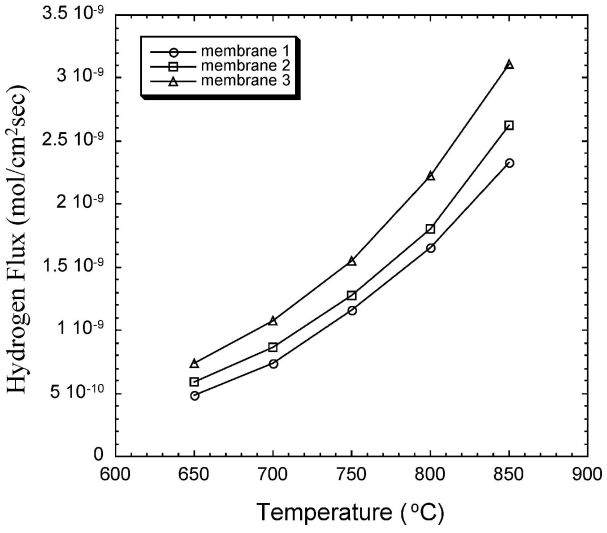

Figure 2 Temperature dependence of the hydrogen flux of three membranes, membrane 1 ball mill for 1 days and sintered at 1773 K for 40 hrs, membrane 2 ball mill for 1 days and sintered at 1773 K for 25 hrs, membrane 3 ball milled for 10 days and sintered at 1773 K for 10 hrs.

dividing the permeation rates by the surface area of the disk membranes. In order to minimize the edge contribution to the permeation, the membrane edge was sealed with ceramic sealant.

Fig. 2 shows the temperature dependence of the hydrogen flux for three membranes prepared by different ways. For all of three membranes, the hydrogen flux increases with temperature over the entire temperature range. As shown in Equation 7, the hydrogen flux may be determined by partial conductivity of electrons and protons. As far as protonic conduction, on the basis of microstructural analysis and electrical characterization by impedance spectroscopy of bulk and single crystal materials, several groups [19, 20, 21] have report that the grain boundaries do not provide a high conductivity pathway for proton conduction. In addition, the total conductivities of the membranes from our AC impedance measurements were equal within experimental errors, Since total conductivity was dominated by proton conductivity within experimental range [13], variation in electron conductivity would not be noticealbe. Therefore, an increase in hydrogen flux with temperature may be caused by electron flow.

Previously, we reported the dopant dependence of hydrogen permeability in strontium cerate (ball milled for 1 days and sintered at 1773 K for 10 hrs) and method to separate electron conductivity from hydrogen flux [22]. Same method can be applied to the membranes prepared in different ways. Fig. 3 shows the hydrogen flux of Eu-doped $SrCeO_{3-\delta}$ (ball milled for 1 days and sintered at 1773 K for 40 hrs) as a function of temperature under various P_{H_2} and P_{H_2O} conditions. For both dry and wet circumstances, hydrogen permeability increases with increasing P_{H_2}.

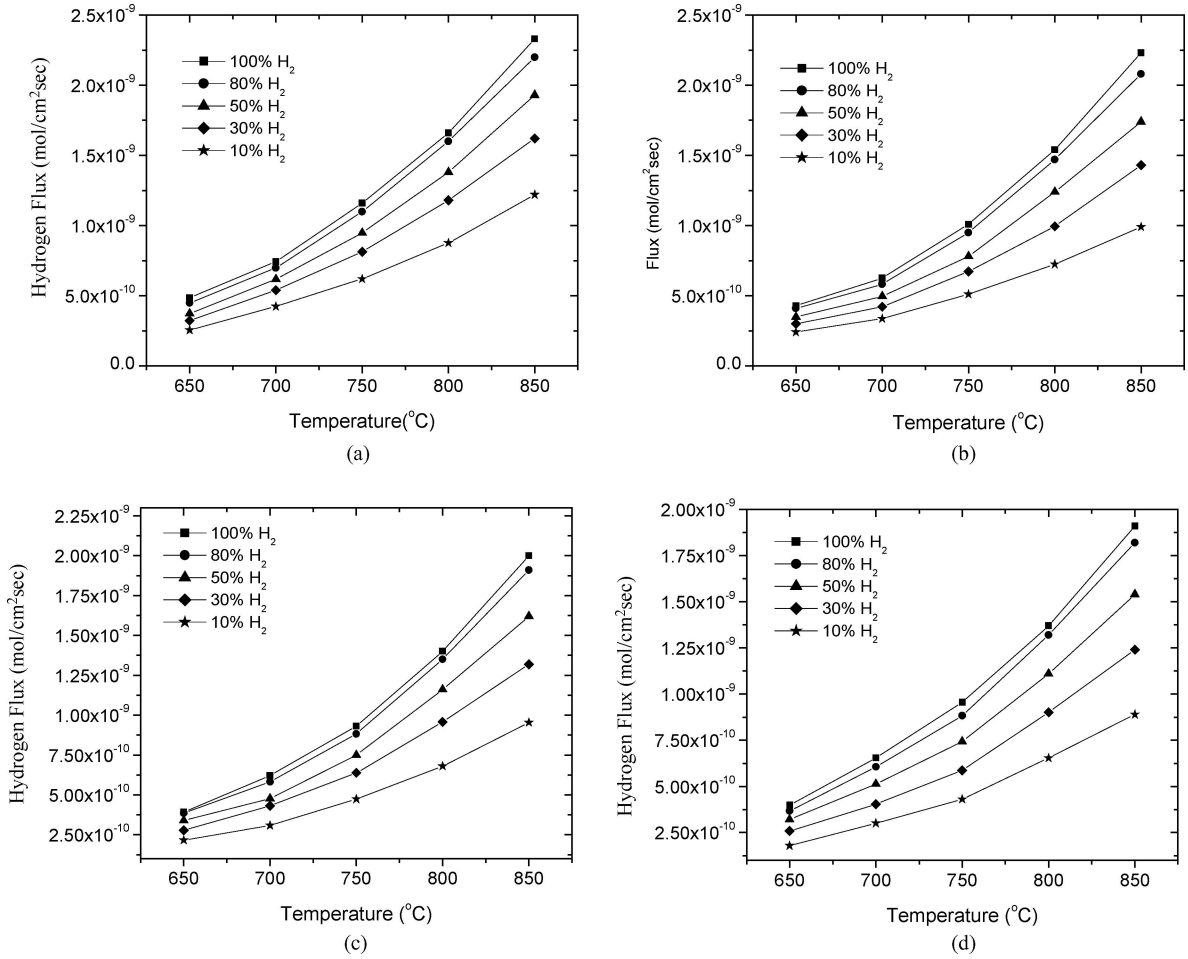

Figure 3 Hydrogen flux as a function of temperature: (a) dry, (b) $pH_2O = 0.028$ atm, (c) $pH_2O = 0.051$ atm, and (d) $pH_2O = 0.086$ atm (the specified hydrogen percents are before bubbling through H_2O).

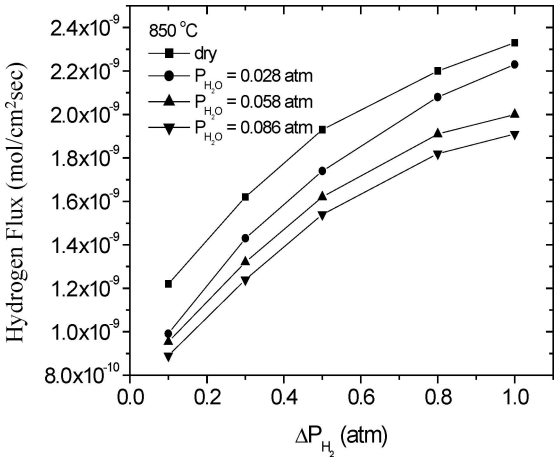

Figure 4 Hydrogen flux as a function of applied hydrogen chemical potential gradients under various pH_2O conditions.

As P_{H_2O} increases as shown in Fig. 4, hydrogen permeability decreases. It can be explained by the change in electron concentration as thermodynamic condition changes. The electronic conductivity decreases with P_{H_2O} because the oxygen chemical potential increases with P_{H_2O}. Therefore, an increase in proton concentration with P_{H_2O} (Equation 4) is simultaneously followed by a decrease in electrons (Equation 3) due to the redox reaction in the oxide membrane.

4.2. Partial conductivities

When both P_{H_2} and P_{H_2O} differences are applied to an oxide membrane, the thermodynamic driving force for hydrogen permeation is not only the P_{H_2} gradient but also the P_{O_2} gradient, as shown in Equation 1. Under our experimental conditions, no discernible oxygen permeation was detected by the mass spectrometer so $t_{v_O^{\cdot\cdot}}$ can be assumed to be zero. Therefore, Equation 1 can be simplified to

$$J_{OH_O^{\cdot}} = -\frac{RT}{2F^2L}\int_{P'_{H_2}}^{P''_{H_2}} \sigma_t t_{OH_O^{\cdot}} t_{e'} d\ln P_{H_2}. \qquad (8)$$

Using Equation 2, we can extract the ambipolar conductivity σ_{amb} from the hydrogen permeation flux as

$$\sigma_{amb} = \frac{\sigma_{OH_O^{\cdot}}\sigma_{e'}}{\sigma_{OH_O^{\cdot}} + \sigma_{e'}} = -\frac{4F^2L}{RT}\left[\frac{\partial J_{H_2}}{\partial \log P''_{H_2}}\right]_{P^{ref}_{H_2}}. \qquad (9)$$

The ambipolar conductivity can be calculated from the slope of the hydrogen permeation flux versus the logarithm of the hydrogen partial pressure. In this calculation, the mean slope at a given P''_{H_2} was determined by using the datum at the P''_{H_2} and interpolation between its nearest neighbors. Fig. 5 shows the calculated ambipolar conductivities of membrane sintered at 1773 K for 40 hrs at various P_{H_2}, P_{H_2O}, and

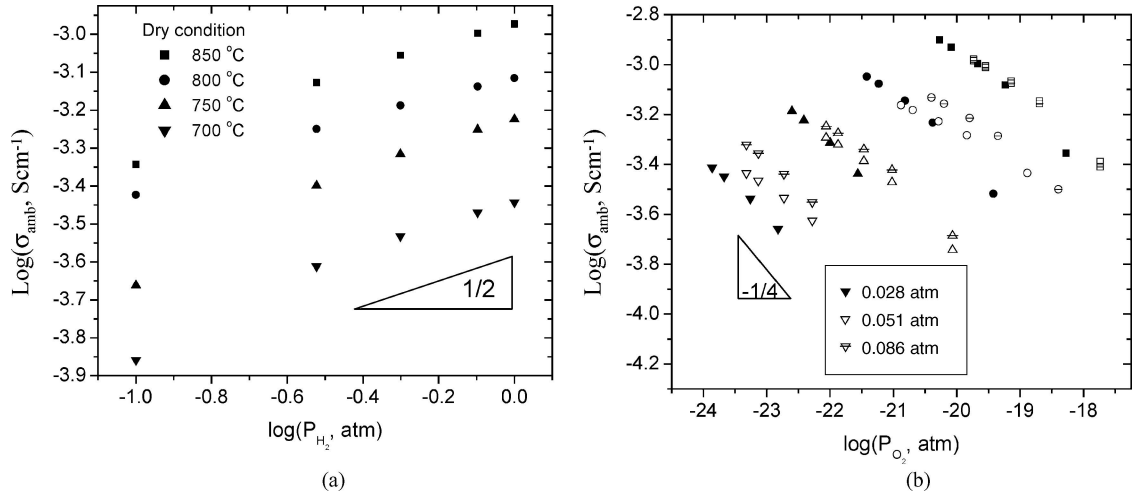

(a) (b)

Figure 5 Ambipolar conductivity as a function of (a) pH_2, and (b) pO_2 (solid symbols: $pH_2O = 0.028$ atm; open symbols: $pH_2O = 0.051$ atm; open symbols with bar: $pH_2O = 0.086$ atm.)

temperatures at a fixed P_{H_2O}. The hydrogen exponent m, $\sigma_{amb} \propto P_{H_2}^m$, takes a value of $\approx 1/2$, as shown in Fig. 5a. The 1/2 slope corresponds to the dependence of electron concentration on hydrogen partial pressure in region, characterized by the charge neutrality condition $2[Eu''_{Ce}] = [OH^{\cdot}_{O}](p < K_A)$,

$$n \propto A' P_{H_2}^{1/2}, \text{ and by } K_{H_2O} = \frac{P_{H_2O}}{P_{O_2}^{1/2} P_{H_2}},$$

$$n \propto A \cdot P_{O_2}^{-1/4} P_{H_2O}^{1/2}, \tag{10}$$

where A and A' are constants that depend on temperature.

The oxygen exponent m, $\sigma_{amb} \propto P_{O_2}^m$, is $\approx -1/4$, as shown in Fig. 5b. The P_{O_2} dependence of hydrogen permeation fluxes within the investigated P_{O_2} range agrees with the P_{O_2} dependence of electrons [13]. To satisfy the P_{H_2} and P_{O_2} dependence of hydrogen permeability, the proton conductivity should still be larger than the electron conductivity so the hydrogen permeability activated by the P_{H_2} and P_{H_2O} differences across the $SrCe_{0.95}Eu_{0.05}O_{3-\delta}$ membrane is controlled by the transport of electrons. The deviations from linearity in Figs 4 and 5 should be noticed and further studied.

The ambipolar conductivity, therefore, can be considered equivalent to the electron conductivity because electrons are still minor charge carriers in the wet reducing atmosphere explored in this experiment, where protons are charge compensated by ionized europium ions. If we assume that $\sigma_{amb} \approx \sigma_{e'}$, the electronic conductivity as a function of temperature is as shown in Fig. 6. The temperature dependence of the electronic conductivity exhibits different behavior for the membranes prepared in different ways. The activation energies determined from the Arrhenius plot under dry condition are ≈0.63 (for the membrane ball milled for 10 days and sintered at 1773 K for 10 hrs), 0.80 eV (for the membrane ball mill for 1 days and sintered at 1773 K for 25 hrs) and 0.83 eV (for the membrane ball mill for 1 days and sintered at 1773 K for 40 hrs), respectively.

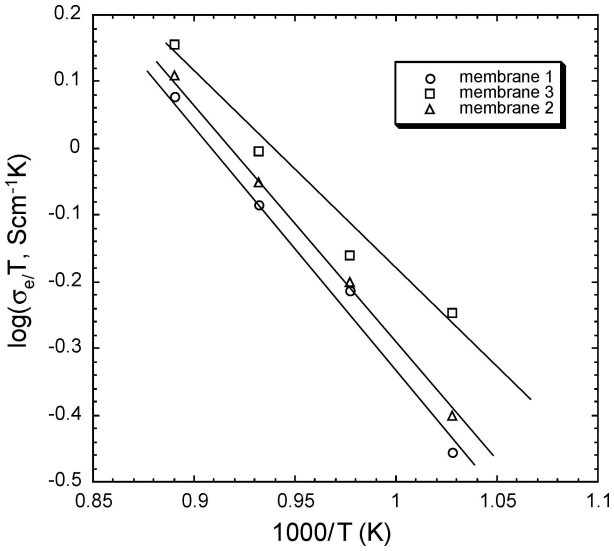

Figure 6 Electronic conductivity as a function of temperature, membrane 1 ball mill for 1 days and sintered at 1773 K for 40 hrs, membrane 2 ball mill for 1 days and sintered at 1773 K for 25 hrs, membrane 3 ball milled for 10 days and sintered at 1773 K for 10 hrs.

The electronic conductivity is found to increase with increasing grain boundary area, or with decreasing grain size when the resistivity of grain boundary is lower that of the grain. Therefore, grain boundaries may provide fast conduction pathway for electrons resulting in enhanced electronic conductivity in smaller grained specimen.

5. Conclusions

Hydrogen permeability of $SrCe_{0.95}Eu_{0.05}O_{3-\delta}$ membranes was studied by measuring gas permeation as a function of temperature and P_{H_2}, and P_{H_2O} gradient. The effect of the microstructure on hydrogen permeability through a 1.72 mm thick membrane was investigated. The ambipolar conductivity calculated from hydrogen permeation fluxes showed the same P_{O_2} and P_{H_2} dependence as the electronic conductivity, for the experimental conditions. The small grained membrane showed higher hydrogen permeability when compared

with the larger grained membrane over the entire temperature range investigated.

Acknowledgments

This work was supported by the U.S. Department of Energy, Office of Fossil Energy, National Energy Technology Laboratory's Gasification Technologies Program, under Contract W-31-109-Eng-38 and NASA, NAG3-2750.

References

1. U. BALACHANDRAN, T. H LEE, S. WANG and S. E. DORRIS, *Inter. J. Hydrogen Energy* **29** (2004) 291.
2. S.-J. SONG, E. D. WACHSMAN, H.-S. YOON and K.-H. LEE, in preparation.
3. R. V. SIRIWARDANE, J. A. POSTER, E. P. FISHER, T. H. LEE, S. E. DORRIS and U. BALACHANDRAN, *App. Surf. Sci.* **167** (2000) 34.
4. U. BALACHANDRAN, B. MAR, P. S. MAIYA, R. L. MIEVILLE, J. T. DUSEK, J. PICCIOLE, J. GUAN, S. E. DORRIS and M. LIU, *Solid State Ionics* **108** (1998) 363.
5. Y. DU and S. NOWICK, *J. Amer. Ceram. Soc* **78** (1995) 3033.
6. P. MARAGARAJ, K. D. KREUER, T. HE, T. SCHOBER and J. MAIER, *Solid State Ionics* **98** (1997) 1.
7. S.-J. SONG, E. D. WACHSMAN, S. E. DORRIS and U. BALACHANDRAN, *Solid State Ionics* **149** (2002) 1.
8. J. RHODES and E. D. WACHSMAN, in Solid State Ionics Devices II-Ceramic Sensor, edited by E. Wachsman, W. Weppner, E. Traversa, M. Liu, P. Vanysek and N. Yamazoe (Electrochem. Soc., (2001) Vol. 200–32, p. 137.
9. H. IWAHARA, *Solid State Ionics* **77** (1995) 289.
10. H. IWAHARA, *Solid State Ionics* **125** (1999) 271.
11. S. M. HAILE, D. A. BOYSEN, C. R. L. CHISHOLM and R. B. MERLE, *Nature* **410** (2001) 910.
12. S.-J. SONG, E. D. WACHSMAN, S. E. DORRIS and U. BALACHANDRAN, *J. Electrochem. Soc.* **150** (2003) A790.
13. S.-J. SONG, E. D. WACHSMAN, S. E. DORRIS and U. BALACHANDRAN, *J. Electrochem. Soc.* **150** (2003) A1484.
14. S.-J. SONG, E. D. WACHSMAN, J. RHODES, S. E. DORRIS and U. BALACHANDRAN, *Solid State Ionics* **164** (2003) 107.
15. F. A. KROGER and V. J. VINK, in Relations Between the Concentrations of Imperfections in Crystalline Solids, Solid State Physics, edited by F. Seitz, D. Turnbull (Academic Press, New York, 1956) Vol. 3, p. 307.
16. G. V. LEWIS and C. R. A. CATLOW, *J. Physics and Chemistry of Solids* **47** (1983) 89.
17. S. HAMAKAWA, L. ANWU and E. IGLESIA, *Solid State Ionics* **148** (2002) 71.
18. T. NORBY and Y. LARRING, *Solid State Ionics* **136** (2000) 139.
19. S. M. HAILE, G. STANEFF and K. H. RYU, *J. Mater. Sci.* **36** (2001) 1149.
20. S. M. HAILE, D. L. WEST and J. CAMPBELL, *J. Mater. Res.* **13** (1998) 1576.
21. A. TSCHOPE, E. SOMMER and R. BIRRINGER, *Solid State Ionics* **139** (2001) 255.
22. S.-J. SONG, E. D. WACHSMAN, J. RHODES, S. E. DORRIS and U. BALACHANDRAN, *Solid State Ionics* **167** (2004) 99.

Received 27 September 2004
and accepted 11 March 2005